Disorder-Induced Ordering in Gallium Oxide Polymorphs

Alexander Azarov,[1,*] Calliope Bazioti,[1] Vishnukanthan Venkatachalapathy,[1,2] Ponniah Vajeeston,[3] Edouard Monakhov,[1] and Andrej Kuznetsov[1,†]

[1]*Department of Physics, Centre for Materials Science and Nanotechnology, University of Oslo, PO Box 1048 Blindern, N-0316 Oslo, Norway*

[2]*Department of Materials Science, National Research Nuclear University, "MEPhI", 31 Kashirskoe Hwy, 115409 Moscow, Russian Federation*

[3]*Department of Chemistry, Centre for Materials Science and Nanotechnology, University of Oslo, PO Box 1033 Blindern, N-0315 Oslo, Norway*

(Received 26 October 2021; accepted 14 December 2021; published 6 January 2022)

Polymorphs are common in nature and can be stabilized by applying external pressure in materials. The pressure and strain can also be induced by the gradually accumulated radiation disorder. However, in semiconductors, the radiation disorder accumulation typically results in the amorphization instead of engaging polymorphism. By studying these phenomena in gallium oxide we found that the amorphization may be prominently suppressed by the monoclinic to orthorhombic phase transition. Utilizing this discovery, a highly oriented single-phase orthorhombic film on the top of the monoclinic gallium oxide substrate was fabricated. Exploring this system, a novel mode of the lateral polymorphic regrowth, not previously observed in solids, was detected. In combination, these data envisage a new direction of research on polymorphs in Ga_2O_3 and, potentially, for similar polymorphic families in other materials.

DOI: 10.1103/PhysRevLett.128.015704

Basic principles of polymorphism in crystals are clear: the lattices adapt to the minimum energy in respect with the temperature and pressure. Meanwhile, controllable stabilization of the metastable phases, e.g., at room temperature, is of great interest because it opts for new properties; however, preferably without applying colossal external pressures [1]. For that matter, reaching metastable conditions via ion beam assisted processes with displaced atoms provoking strain accumulation is an interesting alternative. However, the ion-induced disorder may also result in the amorphization, as it typically occurs in such semiconductors as Si [2] or SiC [3]. Even for so-called "radiation hard" semiconductors, e.g., GaN [4] or ZnO [5], the ion irradiation still ends up with high disorder level or partial amorphization.

Importantly, Ga_2O_3 is well known for its polymorphism [6] and several attempts were recently performed to study the influence of the ion irradiation on the phase stability in Ga_2O_3. For example, Ander *et al.* have detected κ phase in the β-Ga_2O_3 matrix upon heavy ion implants [7], even though the evolution of this process as a function of the implantation parameters has not been explored. More recently, interesting strain accumulation was observed in ion implanted α-Ga_2O_3 [8] and β-Ga_2O_3 [9]. However, the systematic understanding of the disorder-induced ordering in Ga_2O_3 polymorphs was missing in literature. In the present Letter, we use a combination of theoretical and experimental approaches to study the response of β-Ga_2O_3 to ion irradiation exploring a wide range of the experimental parameters, such as type of implanted ions, accumulated dose and irradiation temperature. As a result, we demonstrate controllable ion-beam-induced phase engineering resulting in the formation of the highly oriented κ-phase film on the top of the β-Ga_2O_3 wafer. This breakthrough paves the way for a new synthesis technology and further explorations of the metastable polymorph films and regularly shaped interfaces in the device components not achievable by conventional thin film deposition methods. Thus, the present study, in addition to its fundamental value, may accelerate the technological development of Ga_2O_3, which is one of the most intensively studied ultrawide band gap semiconductor right now [10].

In the present study, (010) and (−201) oriented β-Ga_2O_3 single crystal wafers (Tamura Corp.) were implanted with different ions, specifically $^{58}Ni^+$, $^{69}Ga^+$, and $^{197}Au^+$. Note that most of the data are shown for systematic $^{58}Ni^+$ ion implants, while $^{69}Ga^+$ and $^{197}Au^+$ results are used for comparison to demonstrate the general character of the phenomena. For that reason, the ballistic defect production rates (without accounting for nonlinear cascade density effects [11]) for $^{69}Ga^+$ and $^{197}Au^+$ implants were normalized to that of the $^{58}Ni^+$ ion implanted with 400 keV in a wide dose range of $6 \times 10^{13} - 1 \times 10^{16}$ cm^{-2}. The implantations were performed at room temperature (if not indicated otherwise) and 7° off the normal direction.

The samples were analyzed by a combination of Rutherford backscattering spectrometry in channeling mode (RBS/C), x-ray diffraction (XRD) and scanning

transmission electron microscopy (STEM) combined with electron energy loss spectroscopy (EELS). The RBS/C was performed using 1.6 MeV He^+ ions incident along [010] direction and 165° backscattering geometry. The XRD 2theta measurements were performed using Bruker AXS D8 Discover diffractometer using Cu $K_{\alpha 1}$ radiation in locked-coupled mode.

The STEM and EELS investigations were conducted on an FEI Titan G2 60–300 kV at 300 kV with a probe convergence angle of 24 mrad. The simultaneous STEM imaging was conducted with 3 detectors: high-angle annular dark field (HAADF) (collection angles 101.7–200 mrad), annular dark field (ADF) (collection angles 22.4–101.7 mrad) and annular bright field (ABF) (collection angles 8.5–22.4 mrad). The resulting spatial resolution achieved was approximately 0.08 nm. EELS was performed using a Gatan Quantum 965 imaging filter. The energy dispersion was 0.1 eV/channel and the energy resolution measured using the full width at half maximum (FWHM) of the zero-loss peak was 1.1 eV. Electron transparent TEM samples with a cross-sectional wedge geometry were prepared by mechanical polishing with the final thinning performed by Ar ion milling and plasma cleaning.

The total lattice energies of the Ga_2O_3 polymorphs were calculated applying density functional theory (DFT), as implemented in the VASP code [12]. The interaction between the core (Ga:[Ar] and O:[He]) and the valence electrons were described using the projector-augmented wave (PAW) method [13]. The Perdew, Burke, and Ernzerhof (PBE) [14] gradient corrected functional was used for the exchange-correlation part of the potential for the structural optimization. The large energy cutoff of 600 eV was used to guarantee basis-set completeness. The atoms were deemed to be relaxed when all atomic forces were less than 0.02 eV $Å^{-1}$ and the geometries were assumed to get optimized when the total energy converged to ≤1 meV between two consecutive geometric optimization steps. The crystal lattice parameters for all Ga_2O_3 phases in the equilibrium were computed accordingly and the pressure was applied both isotropically and uniaxially.

Figure 1 summarizes the data proving the ion-beam-induced β-to-κ phase transformation in Ga_2O_3 combining (a) XRD, (b) RBS/C, and (c) STEM measurements of (010) β-Ga_2O_3 samples irradiated with $^{58}Ni^+$ ions. As it is clearly seen from Fig. 1(a) the virgin β-Ga_2O_3 wafer is characterized by a strong reflection around 60.9° attributed to the (020) planes of β-Ga_2O_3. The low dose implants (6×10^{13} and 2×10^{14} Ni/cm^2) result in the formation of the shoulder peak with some oscillations at the high-angle side of the (020) peak. These shoulder peak or oscillations can be attributed to the accumulation of the compressive strain [15] and has been discussed in ion implanted (010) β-Ga_2O_3 [9]. However, further dose increase (1×10^{15} Ni/cm^2) releases this strain and leads to the formation of the broad diffraction peak around 63.4°, which shifts to 63.7° for the dose of 1×10^{16} Ni/cm^2. Importantly, for this highest dose, the strain shoulder peaks practically disappear and the (020) diffraction peak resembles that in the virgin sample. The diffraction peaks centered at 63.4° and 63.7° were interpreted as signatures of the κ-Ga_2O_3 (330) and (060) planes, respectively [16], as systematically analyzed in Fig. S1 in the Supplemental Material-I [17]; notably, Fig. S2 illustrates the evolution in the similarly implanted (−201) β-Ga_2O_3 samples for comparison.

Further insight into the mechanisms of the formation and the integrity of the new phase in Ga_2O_3 can be performed by channeling analysis. Figure 1(b) shows that for the lowest dose sample, the RBS/C spectrum is characterized by the well-resolved Gaussian-like damage peak centered close to the maximum of the nuclear energy loss profile ($R_{pd} = 125$ nm according to the SRIM simulations [24]). The magnitude of this peak is well below the amorphous level that is equivalent to the height of the random spectrum in Fig. 1(b). The increase of the ion dose up to 2×10^{14} cm^{-2} results in the formation of the box-shape disorder layer reaching ∼90% of the random signal. Further dose increase, to 1×10^{15} Ni/cm^2, broadens the disordered layer while the disorder level saturates corroborating with the data for β-Ga_2O_3 obtained previously [25]. Spectacularly, the backscattering yield decreases for the dose of 1×10^{16} Ni/cm^2, implying the lattice ordering along the [010] direction, in agreement with the XRD data revealing (060) the κ-phase diffraction peak. Thus, it can be concluded that the Ga_2O_3 amorphization is suppressed by the β-to-κ phase transition occurring in the implanted region.

To verify the status of this film we performed STEM investigations and Figs. 1(c)–1(h) summarizes the STEM data for the sample implanted with 1×10^{16} Ni/cm^2. Specifically, Fig. 1(c) shows an ABF-STEM image and strain contrast reveals the formation of two distinct regions—the film and the substrate—of the initially homogeneous β-Ga_2O_3 wafer. Selected area electron diffraction (SAED) patterns taken from the unimplanted and implanted regions, i.e., Figs. 1(d) and 1(e), illustrate a prominent transformation from the monoclinic β to ordered orthorhombic κ phase. This phase transformation extends to ∼300 nm from the surface and stops abruptly, forming a sharp interface with the β-phase wafer or substrate, see Fig. 1(c). The contrast associated with defects or strain inside the κ-Ga_2O_3 film gradually increases towards the κ/β interface, see Fig. 1(c). However, fast Fourier transforms (FFTs) from high-resolution images taken at the interfacial area (g) and the upper part (h) of the implanted region show that the ordered orthorhombic phase is retained through the depth of the film as compared with the FFT at the β-Ga_2O_3 substrate, see Fig. 1(f). Thus, SAED and FFTs show the formation of a single-phase ordered orthorhombic κ-phase region both at meso- and

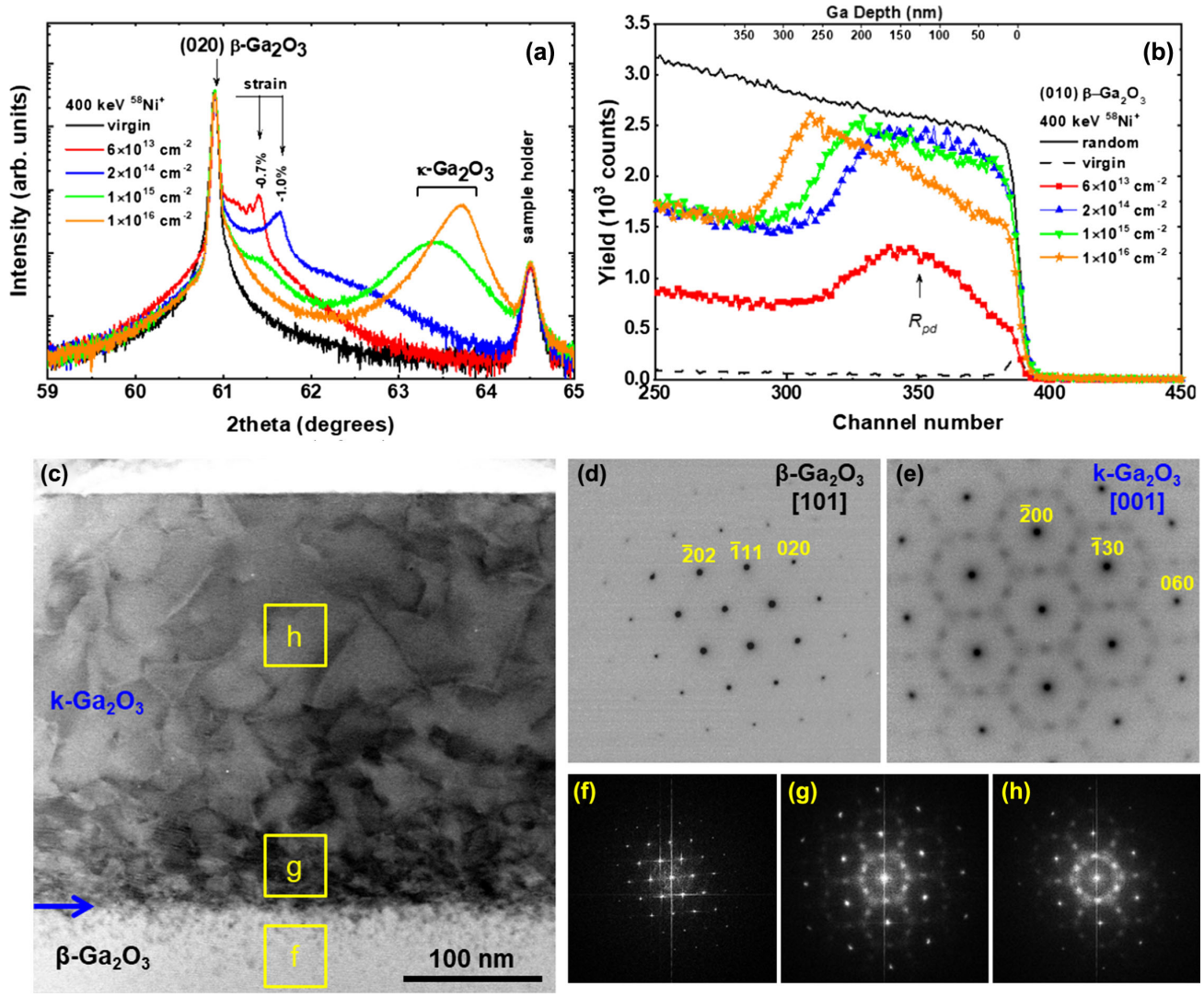

FIG. 1. Ion-beam-induced β-to-κ phase transformation in Ga_2O_3. (a) XRD 2theta scans of the samples implanted with 400 keV $^{58}Ni^+$ ions as a function of ion dose. (b) The corresponding RBS/C spectra with the random and virgin (unimplanted) spectra shown for comparison. The maximum of nuclear energy loss profile (R_{pd}) predicted with SRIM code [24] simulations is shown in correlation with the Ga depth scale. (c) ABF-STEM image of β-Ga_2O_3 sample irradiated with 1×10^{16} Ni/cm^2. Panels (d) and (e) illustrate SAED patterns from the unimplanted and implanted regions, respectively. (f)–(h) FFTs from high-resolution images taken from different regions of the sample as indicated in the panel (c).

nanoscale. The sharp spots, in addition to the lack of extra reflections and/or striking of the main reflections, indicate a highly oriented crystalline film with no signs of high-angle misorientations, high density of misoriented grains or amorphization (see also Fig. S3 in the Supplemental Material II [17]). However, minor misorientations between adjacent grains cannot be excluded, playing a role in the high dechanneling yield in RBS/C and the broadening of the XRD peaks in Fig. 1.

Note that the implanted region in the low dose sample contains only point defects and defect clusters with no indication of the κ phase (see Supplemental Material III [17]). Moreover, the comparison between EELS spectra in Fig. 2 provides additional arguments. Indeed, because of different atomic coordination in β and κ phases we detected characteristic changes in the fine structure of the EELS spectra acquired in the STEM mode, by comparing low and high-dose implanted samples. In particular, the oxygen K edge is characterized by two main peaks, labeled A and B in Fig. 2, related to the O $2p$–Ga $4s$ and O $2p$–Ga $4p$ bonding, respectively. As seen from Fig. 2, prominent changes in the A/B intensity ratio (I_A/I_B) occur when the phase transition takes place. Specifically, I_A/I_B decreases in the κ phase. This can be attributed either to the increase in O $2p$–Ga $4p$ hybridization or to the transfer of electrons from O $2p$–Ga $4p$ band into another band [7,26].

It should be emphasized that the phenomenon of the β-to-κ phase transition is generically related to the

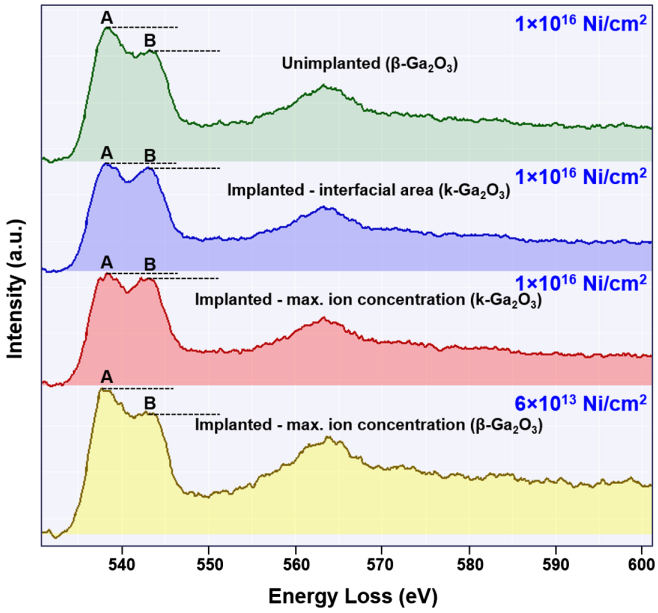

FIG. 2. EELS spectra of the oxygen K edge, acquired from different areas of the high-dose and low-dose implanted β-Ga_2O_3, illustrating characteristic intensity changes correlated with β-to-κ transition.

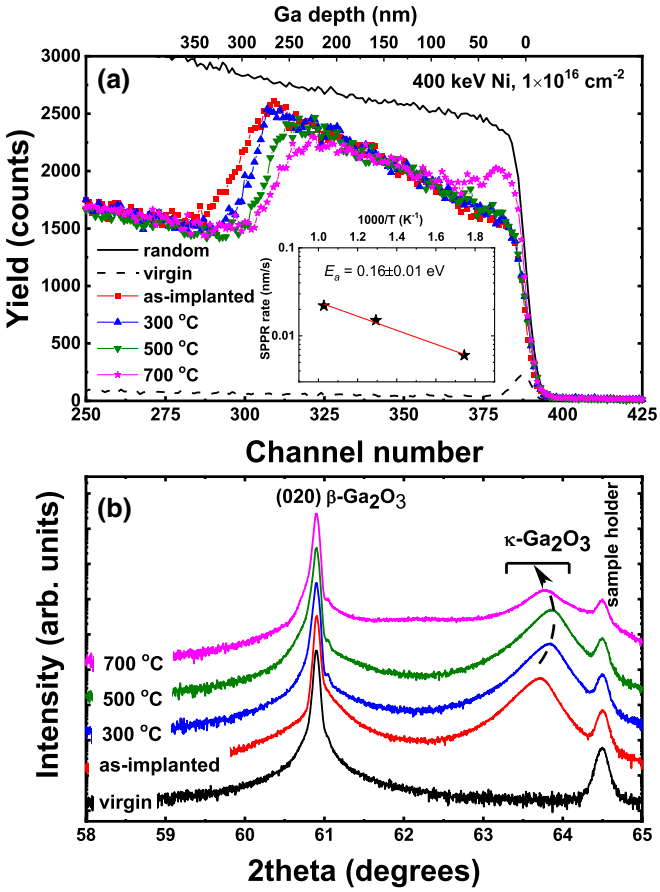

FIG. 3. Thermal stability of the ion-beam-induced κ-Ga_2O_3 film. (a) RBS/C spectra and (b) corresponding XRD 2theta scans of the sample shown in Fig. 1(c) before and after isochronal anneals as indicated in the legend. The inset in the panel (a) shows an Arrhenius plot of the solid-phase polymorphic regrowth rate as deduced from the RBS/C data.

accumulation of the lattice disorder and not to the chemical nature of the implanted ions. This was proved by performing control implants with Ga and Au ions (see Figs. S1 and S5 in the Supplemental Material I and IV [17]).

Further, we investigated the thermal stability of the formed κ-Ga_2O_3 film. The RBS/C data show that the anneals at 300 °C–700 °C result in the reduction of the κ-film thickness as revealed by the shifts of the RBS/C spectra in the range corresponding to the β/κ interface region [Fig. 3(a)]. However, increasing the temperature to 700 °C enhances the yield in the near surface region, indicating the disintegration of the κ-phase film. The corresponding XRD data in Fig. 3(b) show that the (060) κ-phase peak position shifts too and for 300 °C–500 °C it moves towards better fits with literature data [16]. This shift may indicate an improvement of the κ-Ga_2O_3 phase crystallinity because of annealing of the misoriented grains and relaxation of the enhanced strain (see Supplemental Material V [17]) at the β/κ interface region consistently with the RBS/C data in Fig. 3(a).

Moreover, based on the data in Fig. 3, lateral solid-phase regrowth of the polymorphs can be emphasized. The kinetics of this process resembles that of the solid phase epitaxial regrowth of the amorphous phase induced by ion irradiation, e.g., for amorphous silicon [2], even though in reality Fig. 3 reveals the crystalline phase transition. The inset in Fig. 3(a) plots the rate of this process as a function of the annealing temperature, revealing the activation energy of 0.16 ± 0.1 eV. Notably, in accordance with literature [27] κ-Ga_2O_3 deposited with conventional techniques starts to degrade at ~650 °C, but the nucleation of the β phase occurs in the bulk of the κ-phase layer. Thus, our results suggest an important role of the β/κ interface for the thermal stability of radiation-induced κ-Ga_2O_3 films.

The fundamental reason of the κ-phase metastability is of a thermodynamic origin and we analyzed Ga_2O_3 phases using DFT. Figure 4 shows the total energy for α-, β-, and κ-Ga_2O_3 lattices subjected to isotropic or uniaxial pressure, plotted as a function of volume per formula unit (f.u.) for two different intervals in panels (a) and (b). Notably, there are more Ga_2O_3 polymorphs available, however the α, β, and κ phases are the lowest in energy as seen from Fig. S7 in the Supplemental Material VI [17]. In particular, the κ phase exhibits its energy minimum closest to that of the β phase, making the β-to-κ transition likely to occur as soon as sufficient strain is provided (~2%, corresponding to the volume of ~51.35 $Å^3$/f.u. in Fig. 4 for isotropic pressure and strain). Thus, we believe that such strain conditions are gradually reached by the high dose implants, finally resulting in the κ-phase film. Meanwhile, the strain

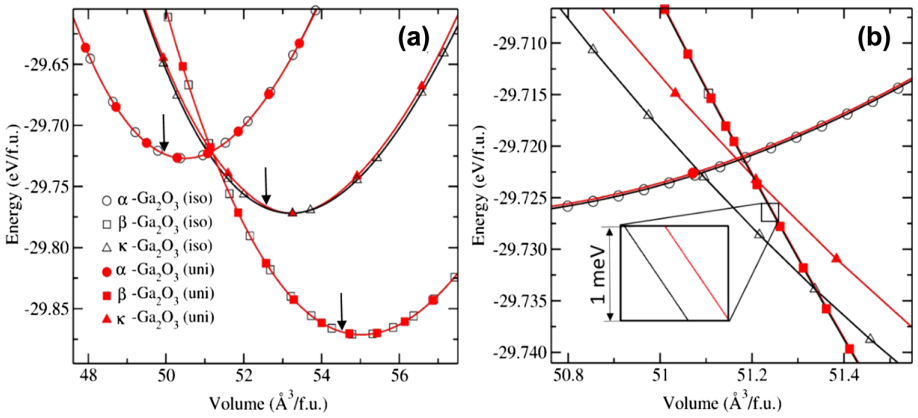

FIG. 4. DFT calculated lattice energies for α-, β-, and κ-Ga_2O_3 as a function of the volume per formula unit for (a) bigger interval showing energy minima for the corresponding phases and (b) smaller interval emphasizing the transition points. The data were collected under isotropic (open symbols) and uniaxial stress along the [010] direction (solid symbols). Experimental volumes of different phases are indicated by the arrows.

sufficient to ignite β-to-α phase transition is only slightly higher, see Fig. 4(a); meaning that the formation of the α phase is also possible, as was also experimentally demonstrated under high isotropic pressure [28]. To start this process, there is an additional activation volume to overcome (as compared to β-to-κ transition), since the energy minima for the α phase corresponds to the volume of $\sim$50.5 Å^3/f.u. in Fig. 4(a). This explains the reason of the single-phase κ film in Fig. 1(c) instead of the α/κ-phase mixture or α phase alone. Thus, the scenario behind the observations in Figs. 1 and 2 is consistent the theoretical predictions of the radiation disorder-induced strain reaching a threshold to ignite the β-to-κ transition and, consequently, relaxing the strain by moving the system to the κ-phase energy minimum in Fig. 4(a).

Notably, Fig. 4 also compares the isotropic and uniaxial pressures, since at present we do not have sufficient experimental arguments to conclude on the strain distribution. Nonisotropic strain conditions are realistic because of the preferential localizations of the radiation defects and building defect complexes with specific configurations [29], likely compressing or stretching certain crystal directions. Nevertheless, for the pressures applied, nonnegligible energy difference, as compared with the isotropic strain, occurs in κ-Ga_2O_3 only, see Fig. 4(b). Interestingly, it shifts the κ-Ga_2O_3 energy curve towards the "triple point" intersection for the α, β, and κ phases at the volume of $\sim$51.2 Å^3/f.u. in Fig. 4(b). An additional important parameter not taken into account in Fig. 4 is temperature. Indeed, the data in Fig. 4 represent the ground state only, while the temperature shifts the stability range for all phases as illustrated in Fig. S11 in the Supplemental Material VI [17]. Moreover, temperature might affect the balance between migration and annihilation of the radiation-induced defects [9], making it to an important factor for the localization of the β/κ interface in respect to the R_{pd} region (see Fig. S12 in the Supplemental Material VII [17]).

In conclusion, we have studied ion-induced phase transitions in β-Ga_2O_3. The mechanism involves the lattice disorder-induced strain accumulation that ignites the transition upon reaching sufficient strain threshold as predicted by theory. As a result, we fabricated the [010] oriented orthorhombic κ-phase film on the top of the [010] oriented monoclinic β-phase substrate, demonstrating sharp κ/β interface not previously realized by conventional thin film deposition methods. We also observed a novel mode of the solid-phase polymorphic regrowth of the β phase on the expense of the κ phase maintained across the lateral κ/β interface and exhibiting the activation energy of 0.16 ± 0.1 eV at 300 °C–500 °C. In combination, the present work paves the way for further development of the polymorph films and interfaces by ion beam fabrication, envisaging this new research direction for Ga_2O_3 and, potentially, for similar polymorphic families in other materials.

This work was performed within the Research Centre for Sustainable Solar Cell Technology (FME SuSolTech, Project No. 257639) co-sponsored by the Research Council of Norway and industry partners. The Research Council of Norway is acknowledged for the support to the Norwegian Micro- and Nano-Fabrication Facility, NorFab, Project No. 295864, and to the Norwegian Center for Transmission Electron Microscopy, NORTEM, Project No. 197405/F50. We also acknowledge the Research Council of Norway for providing the computer time, Projects No. NN2875k and No. NS2875k) at the Norwegian Supercomputer Facility. The INTPART Program at the Research Council of Norway, Projects No. 261574 and No. 322382, enabled the international collaboration.

*Corresponding author.
alexander.azarov@smn.uio.no
†Corresponding author.
andrej.kuznetsov@fys.uio.no

[1] Q. Y. Hu, J.-F. Shu, A. Cadien, Y. Meng, W. G. Yang, H. W. Sheng, and H.-K. Mao, Polymorphic phase transition mechanism of compressed coesite, Nat. Commun. **6**, 6630 (2015).
[2] F. Priolo and E. Rimini, Ion-beam-induced epitaxial crystallization and amorphization in silicon, Mater. Sci. Rep. **5**, 321 (1990).
[3] A. Debelle, A. Boulle, A. Chartier, F. Gao, and W. J. Weber, Interplay between atomic disorder, lattice swelling, and defect energy in ion-irradiation-induced amorphization of SiC, Phys. Rev. B **90**, 174112 (2014).
[4] M. C. Sequeira, J.-G. Mattei, H. Vazquez, F. Djurabekova, K. Nordlund, I. Monnet, P. Mota-Santiago, P. Kluth, C. Grygiel, S. Zhang, E. Alves, and K. Lorenz, Unravelling the secrets of the resistance of GaN to strongly ionising radiation, Commun. Phys. **4**, 51 (2021).
[5] A. Yu. Azarov, A. Hallén, P. Rauwel, X. L. Du, A. Yu. Kuznetsov, and B. G. Svensson, Effect of implanted species on thermal evolution of ion-induced defects in ZnO, J. Appl. Phys. **115**, 073512 (2014).
[6] H. Y. Playford, A. C. Hannon, E. R. Barney, and R. I. Walton, Structures of uncharacterised polymorphs of Gallium Oxide from total neutron diffraction, Chem. Eur. J. **19**, 2803 (2013).
[7] E. A. Anber, D. Foley, A. C. Lang, J. Nathaniel, J. L. Hart, M. J. Tadjer, K. D. Hobart, S. Pearton, and M. L. Taheri, Structural transition and recovery of Ge implanted β-Ga_2O_3, Appl. Phys. Lett. **117**, 152101 (2020).
[8] D. Tetelbaum, A. Nikolskaya, D. Korolev, T. Mullagaliev, A. Belov, V. Trushin, Y. Dudin, A. Nezhdanov, A. Mashin, A. Mikhaylov, A. Pechnikov, M. Scheglov, V. Nikolaev, and D. Gogova, Ion-beam modification of metastable gallium oxide polymorphs, Mater. Lett. **302**, 130346 (2021).
[9] A. Azarov, V. Venkatachalapathy, E. V. Monakhov, and A. Yu. Kuznetsov, Dominating migration barrier for intrinsic defects in gallium oxide: Dose-rate effect measurements, Appl. Phys. Lett. **118**, 232101 (2021).
[10] S. J. Pearton, J. Yang, P. H. Cary, F. Ren, J. Kim, M. J. Tadjer, and M. A. Mastro, A review of Ga_2O_3 materials, processing, and devices, Appl. Phys. Rev. **5**, 011301 (2018).
[11] J. B. Wallace, L. B. Bayu Aji, L. Shao, and S. O. Kucheyev, Deterministic Role of Collision Cascade Density in Radiation Defect Dynamics in Si, Phys. Rev. Lett. **120**, 216101 (2018).
[12] G. Kresse and J. Furthmüller, Efficient iterative schemes for ab initio total-energy calculations using a plane-wave basis set, Phys. Rev. B **54**, 11169 (1996).
[13] P. E. Blöchl, Projector augmented-wave method, Phys. Rev. B **50**, 17953 (1994).
[14] J. P. Perdew, K. Burke, and M. Ernzerhof, Generalized Gradient Approximation Made Simple, Phys. Rev. Lett. **77**, 3865 (1996).
[15] A. Debelle and A. Declémy, XRD investigation of the strain/stress state of ion-irradiated crystals, Nucl. Instrum. Methods Phys. Res., Sect. B **268**, 1460 (2010).
[16] I. Cora, F. Mezzadri, F. Boschi, M. Bosi, M. Čaplovičová, G. Calestani, I. Dódony, B. Pécz, and R. Fornari, The real structure of ε-Ga_2O_3 and its relation to κ-phase, Cryst. Eng. Commun. **19**, 1509 (2017).
[17] See Supplemental Material at http://link.aps.org/supplemental/10.1103/PhysRevLett.128.015704 for additional experimental and theoretical results, which includes additional Refs. [18–23].
[18] S. Yoshioka, H. Hayashi, A. Kuwabara, F. Oba, K. Matsunaga, and I. Tanaka, Structures and energetics of Ga_2O_3 polymorphs, J. Phys. Condens. Matter. **19**, 346211 (2007).
[19] A. I. Titov, A. Yu. Azarov, L. M. Nikulina, and S. O. Kucheyev, Damage buildup and the molecular effect in Si bombarded with PFn cluster ions, Nucl. Instrum. Methods Phys. Res., Sect. B **256**, 207 (2007).
[20] A. Togo, F. Oba, and I. Tanaka, First-principles calculations of the ferroelastic transition between rutile-type and $CaCl_2$-type SiO_2 at high pressures, Phys. Rev. B **78**, 134106 (2008).
[21] H. J. Monkhorst and J. D. Pack, Special points for Brillouin-zone integrations, Phys. Rev. B **13**, 5188 (1976).
[22] H. Wang, Y. He, W. Chen, Y. W. Zeng, K. Stahl, T. Kikegawa, and J. Z. Jiang, High-pressure behavior of β-Ga_2O_3 nanocrystals, J. Appl. Phys. **107**, 033520 (2010).
[23] K. E. Lipinska-Kalita, P. E. Kalita, O. A. Hemmers, and T. Hartmann, Equation of state of gallium oxide to 70 GPa: Comparison of quasihydrostatic and nonhydrostatic compression, Phys. Rev. B **77**, 094123 (2008).
[24] J. F. Ziegler, M. D. Ziegler, and J. P. Biersack, SRIM—the stopping and range of ions in matter (2010), Nucl. Instrum. Methods Phys. Res., Sect. B **268**, 1818 (2010).
[25] E. Wendler, E. Treiber, J. Baldauf, S. Wolf, and C. Ronning, High-level damage saturation below amorphisation in ion implanted β-Ga_2O_3, Nucl. Instrum. Methods Phys. Res., Sect. B **379**, 85 (2016).
[26] A. Sharma, M. Varshney, H.-J. Shin, K. H. Chae, and S. O. Won, Investigation on cation distribution and luminescence in spinel phase γ-$Ga_{3-\delta}O_4$: Sm nanostructures using X-ray absorption spectroscopy, RSC Adv. **7**, 52543 (2017).
[27] I. Cora, Zs. Fogarassy, R. Fornari, M. Bosi, A. Rečnik, and B. Pécz, In situ TEM study of $\kappa \rightarrow \beta$ and $\kappa \rightarrow \gamma$ phase transformations in Ga_2O_3, Acta Mater. **183**, 216 (2020).
[28] D. Machon, P. F. McMillan, B. Xu, and J. Dong, High-pressure study of the β-to-α transition in Ga_2O_3, Phys. Rev. B **73**, 094125 (2006).
[29] M. E. Ingebrigtsen, A. Yu. Kuznetsov, B. G. Svensson, G. Alfieri, A. Mihaila, U. Badstübner, A. Perron, L. Vines, and J. B. Varley, Impact of proton irradiation on conductivity and deep level defects in β-Ga_2O_3, APL Mater. **7**, 022510 (2019).